PHYSICAL REVIEW C VOLUME 1, NUMBER 6 JUNE 1970

Energy Dependence of ^{22}Na and ^{24}Na Production Cross Sections with 100- to 400-MeV Protons*

Ralph G. Korteling
Department of Chemistry, Simon Fraser University, Burnaby, British Columbia
and
Albert A. Caretto, Jr.
Department of Chemistry, Carnegie-Mellon University, Pittsburgh, Pennsylvania 15213
(Received 27 January 1969; revised manuscript received 31 December 1969)

Cross sections for the production of ^{22}Na and ^{24}Na have been determined from targets between magnesium ($Z=12$) and selenium ($Z=34$) with 100-, 200-, and 300-MeV protons. The main feature of the results is the exponential decrease of the cross sections with increasing target atomic number or neutron number for values up to $Z\simeq 30$ and $N\simeq 37$. This feature has been found to be consistent with the cross-section dependence predicted on the basis of a cascade-evaporation mechanism. Maxima are also observed in the cross-section distributions at atomic numbers greater than $Z=30$. It appears that these maxima are caused by nonconventional cascade-evaporation events, since they have thresholds below 200 MeV. A major breakup process in which one of the fragments has greater stability is suggested as a possible mechanism.

INTRODUCTION

Cross sections for the production of ^{22}Na and ^{24}Na with 400-MeV protons from 36 different target elements having atomic numbers less than 50 have been reported recently.[1] These cross sections decrease exponentially as a function of atomic number of the target or the neutron number of the target. The exponential dependence of the cross sections on target atomic number was interpreted[1] in terms of the conventional cascade-evaporation model of high-energy nuclear interactions with complex nuclei. Deviations from this exponential dependence were observed for elements with atomic numbers greater than 30, and in fact, cross-section maxima were observed for atomic numbers equal to about 33 and 45. The over-all gross ^{24}Na cross-section dependence on Z was found to be in agreement with the results of previous workers.[2,3]

The energy dependence of the exponential decrease in cross section, as a function of target, is of growing interest. Analytical representations of the production cross sections[4] for spallation products have been shown to be quite useful in predicting unknown values. Experimental data, on which the various parameters for the expressions are based, are needed in the lower mass and energy region. The study of the production of Na isotopes from a series of targets as a function of energy can yield a good measure of the energy-dependence parameter used in these functions. In addition, the data can be used to check the agreement of existing expressions and parameters in this energy and mass region.

The energy dependence in the region of Z equal to 33 to 45 is also of considerable interest. The possibility that contaminants might be at least partially responsible for the observed structure can be ruled out most definitely by observing the energy dependence in those regions of target Z suspected of impurity problems.

For these reasons a systematic study of the production cross sections of ^{22}Na and ^{24}Na at proton energies between 100–400 MeV was undertaken.

EXPERIMENTAL PROCEDURE

The experimental procedures were similar to those previously described.[1,5] The elements which were bombarded are given in Table I together with their target characteristics. The targets were irradiated in the internal proton beam of the Carnegie-Mellon University 440-MeV synchrocyclotron using standard techniques of energy selection and beam-current determination. Three energies of 100, 200, and 300 MeV were selected for these irradiations and were believed to be correct to ±10 MeV. The proton beam was monitored by the ^{27}Al(p, $3pn$)^{24}Na and ^{27}Al(p, $3p3n$)^{22}Na reactions. The monitor cross sections are given in Table II.

The target elements (see Table I) were high-purity metal foils whenever possible. Otherwise, the elements were bombarded as inorganic salts in self-supporting pellets. The pellets were formed by mixing spectroscopically pure boric acid with the salt, and then compressing the mixture with pressures of up to 45 tons/in.^{2}.

TABLE I. Target characteristics.

Z	Symbol	Form	Composition	Purity[a]	Activity measurement
12	Mg	pellet	90% H_3BO_3, 10% MgO	Spec	γ
13	Al	foil	metallic	99.99%	β,γ
14	Si	pellet	80% H_3BO_3, 20% SiO_2	Spec	γ
15	P	pellet	80% H_3BO_3, 20% KH_2PO_4	Spec	γ
16	S	pellet	80% H_3BO_3, 20% $(NH_4)_2SO_4$	Spec	γ
17	Cl	pellet	80% H_3BO_3, 20% NH_4Cl	Spec	γ
19	K	pellet	80% H_3BO_3, 20% K_2CO_3 also KBr	Spec	β,γ
20	Ca	pellet	80% H_3BO_3, 20% $CaCO_3$	Spec	γ
21	Sc	pellet	80% H_3BO_3, 20% Sc_2O_3	Spec	γ
22	Ti	foil	metallic	99.7%	β,γ
23	V	foil	metallic	99.8%	β,γ
24	Cr	pellet	80% H_3BO_3, 20% Cr_2O_3	Spec	γ
25	Mn	pellet	80% H_3BO_3, 20% Mn_3O_4	Spec	β,γ
26	Fe	foil	metallic	99.9%	β,γ
27	Co	foil	metallic	99.8%	β,γ
28	Ni	foil	metallic	99.5%	β,γ
29	Cu	foil	metallic	99.5%	β,γ
30	Zn	foil	metallic	99.9%	β,γ
31	Ga	pellet	80% H_3BO_3, 20% Ga_2O_3	Spec	β
32	Ge	pellet	80% H_3BO_3, 20% GeO_2	Spec	β
33	As	pellet	80% H_3BO_3, 20% As_2O_3	Spec	β
34	Se	pellet	80% H_3BO_3, 20% SeO_2	Spec	β

[a]Spec = spectroscopically pure.

The targets themselves consisted of a stack of the various foils or pellets clamped on a probe head. The order, as exposed to the beam, was: 3-mil Al guard foil, 1-mil Al (99.99%) monitor, 1-mil Al guard foil, an inert guard foil, target-element foils or pellets, another inert guard foil, and then another set of Al monitor foils. The pellet targets were separated from each other and the monitor foils by 3-mil Mylar. The metal foils were chosen in groups of similar atomic number and were placed in order of decreasing Z value. Generally four metal foils or two pellets were bombarded at the same time giving a mass of 200 -300 mg/cm^2 for the total stack. Special care was taken to maintain alignment of the stack. This was checked experimentally by comparing the activity of the front and back Al monitor foils. The two activities generally agreed within 1% of each other and very rarely exceeded 3%. An average number was taken for a beam measurement.

The target elements Mg through Sc were mounted directly for counting without performing any radiochemical separations. For target elements of atomic number >21, the sodium activities were separated by standard radiochemical means prior to counting. The procedure followed has been described previously.[1] Chemical yields were determined to within 5%.

The ^{24}Na production was determined by counting its 2.76-MeV γ ray by using 3-in.×3-in. NaI crystals coupled to multichannel analyzers. For the target elements of Z greater than scandium which required radiochemical separation, the ^{24}Na activity was measured by determination of either the 15-h β decay, or the 2.76-MeV γ ray. Standard gas-flow, end-window β proportional counters were used for the β-activity measurements. In all cases the activity was measured relative to the aluminum-monitor activity, and therefore only a nominal 2% uncertainty generally need be assigned to these measurements. However, in the cases where extremely low ^{24}Na production cross sections were combined with low-beam-density requirements because of target characteristics (i.e., Ge to As at 100 MeV), larger uncertainty limits need to be given as a result of low counting rates and the possibility of undetectable target misalignment.

The ^{22}Na activity was determined by measuring the 1.28-MeV γ transition, or the β^+ emission in either a β-proportional counter or a 511–511-KeV coincidence counter. Because of the lower count rate, the measurements of ^{22}Na have a larger error than those for ^{24}Na.

RESULTS

The experimental cross sections for the production of ^{22}Na and ^{24}Na from targets with atomic num-

TABLE II. Experimental production cross sections (mb).

Target element Atomic number	Symbol	^{22}Na		^{24}Na	
		100-MeV incident protons			
11	Na	54.9 ±1.7[a]	(2)[b]	...	...
12	Mg	38.9 ±3.1	(2)	5.30 ±0.63[a]	(2)[b]
13	Al[c]	15.5	...	10.2	...
14	Si	14.5 ±0.9	(3)	2.92 ±0.14	(3)
15	P	4.90 ±0.29	(2)	3.98 ±<0.01	(2)
16	S	4.08 ±0.28	(2)	1.01 ±0.13	(2)
17	Cl	0.649 ±0.084	(2)	0.669 ±0.053	(2)
19	K	(8.39 ±0.50) $\times10^{-2}$	(2)	(4.46 ±0.07) $\times10^{-2}$	(2)
20	Ca	...	...	(1.59 ±0.76) $\times10^{-2}$	(3)
21	Sc	(7.30 ±1.40) $\times10^{-2}$	(2)	(6.60 ±0.30) $\times10^{-2}$	(2)
22	Ti	(1.48 ±0.02) $\times10^{-2}$	(2)	(1.00 ±0.06) $\times10^{-2}$	(2)
23	V	(1.77 ±0.03) $\times10^{-2}$	(2)	(5.96 ±0.59) $\times10^{-3}$	(2)
25	Mn	(9.8 ...) $\times10^{-3}$	(1)	(5.84 ±4.6) $\times10^{-3}$	(2)
26	Fe	(3.21 ±0.12) $\times10^{-3}$	(2)	(1.57 ±0.03) $\times10^{-3}$	(2)
27	Co	(4.98 ±0.11) $\times10^{-3}$	(3)	(1.48 ±0.14) $\times10^{-3}$	(3)
28	Ni	(1.71 ±0.50) $\times10^{-3}$	(3)	(7.98 ±3.1) $\times10^{-4}$	(3)
29	Cu	(1.36 ±0.54) $\times10^{-3}$	(3)	(5.08 ±0.64) $\times10^{-4}$	(3)
30	Zn	(1.71 ±0.17) $\times10^{-3}$	(3)	(4.18 ±0.57) $\times10^{-4}$	(2)
31	Ga	(7.0 ±5.0) $\times10^{-3}$	(2)	(2.0 ±2.0) $\times10^{-4}$	(2)
32	Ge	(3.0 ±3.0) $\times10^{-3}$	(2)	(2.0 ±2.0) $\times10^{-4}$	(2)
33	As	<1.0 $\times10^{-3}$	(2)	<1.0 $\times10^{-4}$	(2)
34	Se	<1.0 $\times10^{-3}$	(2)	<1.0 $\times10^{-4}$	(2)
		200-MeV incident protons			
11	Na	44.2 ±4.3[a]	(2)[b]	(4.65 ±0.69)[a] $\times10^{-2}$	(2)[b]
12	Mg	32.7 ±0.1	(2)	4.38 ±0.11	(2)
13	Al[c]	15.5	...	9.3	...
14	Si	16.1 ±0.40	(3)	3.33 ±0.10	(3)
15	P	8.01 ±0.28	(4)	4.91 ±0.15	(4)
16	S	7.36 ±0.15	(3)	2.20 ±0.08	(3)
17	Cl	2.60 ±0.05	(2)	2.14 ±0.05	(2)
19	K	0.691 ±0.019	(3)	0.538 ±0.011	(3)
20	Ca	0.606 ±0.028	(3)	0.343 ±0.002	(4)
21	Sc	0.17 ...	(1)	0.24 ...	(1)
22	Ti	(5.04 ±0.28) $\times10^{-2}$	(2)	(6.82 ±0.01) $\times10^{-2}$	(2)
23	V	(3.40 ±0.05) $\times10^{-2}$	(2)	(3.78 ±0.04) $\times10^{-2}$	(2)
26	Fe	(1.64 ±0.07) $\times10^{-2}$	(2)	(1.29 ±0.03) $\times10^{-2}$	(2)
27	Co	(1.09 ±0.01) $\times10^{-2}$	(2)	(9.12 ±0.27) $\times10^{-3}$	(2)
28	Ni	(1.10 ±0.03) $\times10^{-2}$	(2)	(5.91 ±0.09) $\times10^{-3}$	(2)
29	Cu	(5.25 ±0.17) $\times10^{-3}$	(2)	(5.46 ±0.20) $\times10^{-3}$	(2)
30	Zu	(8.04 ±0.57) $\times10^{-3}$	(2)	(4.61 ±0.16) $\times10^{-3}$	(2)
31	Ga	(6.0 ±6.0) $\times10^{-2}$	(2)	(2.47 ±1.8) $\times10^{-3}$	(2)
32	Ge	(4.9 ±1.5) $\times10^{-2}$	(2)	(5.57 ±1.0) $\times10^{-3}$	(2)
33	As	(9.5 ±4.3) $\times10^{-3}$	(2)	(7.63 ±0.34) $\times10^{-3}$	(2)
34	Se	(6.0 ±6.0) $\times10^{-3}$	(2)	(1.66 ±0.72) $\times10^{-3}$	(2)
		300-MeV incident protons			
11	Na	37.7 ±1.5[a]	(3)[b]	(6.03 ±1.2)[a] $\times10^{-2}$	(3)[b]
12	Mg	31.0 ±0.8	(2)	4.65 ±0.06	(2)
13	Al[c]	15.5	...	10.1	...
14	Si	20.8 ±0.68	(3)	4.65 ±0.04	(3)
15	P	8.42 ±0.92	(5)	5.53 ±0.26	(4)
16	S	9.05 ±0.10	(2)	3.06 ±0.07	(3)
17	Cl	3.84 ±0.03	(3)	3.03 ±0.08	(3)
19	K	1.40 ±0.11	(4)	1.10 ±0.05	(4)
20	Ca	1.57 ±0.13	(4)	0.784 ±0.012	(4)
21	Sc	0.58 ...	(1)	0.60 ...	(1)

TABLE II (*Continued*)

22	Ti	0.149 ± 0.011	(2)	0.237 ± 0.005	(2)
23	V	(7.16 ± 0.64) $\times 10^{-2}$	(2)	0.125 ± 0.010	(2)
26	Fe	(4.50 ± 0.23) $\times 10^{-2}$	(2)	(4.84 ± 0.02) $\times 10^{-2}$	(2)
27	Co	(2.88 ± 0.01) $\times 10^{-2}$	(2)	(3.50 ± 0.001) $\times 10^{-2}$	(2)
28	Ni	(4.46 ± 0.88) $\times 10^{-2}$	(2)	(2.48 ± 0.005) $\times 10^{-2}$	(2)
29	Cu	(1.51 ± 0.06) $\times 10^{-2}$	(2)	(1.98 ± 0.05) $\times 10^{-2}$	(2)
30	Zn	(1.46 ± 0.02) $\times 10^{-2}$	(2)	(1.69 ± 0.03) $\times 10^{-2}$	(2)
31	Ga	(2.60 ± 0.51) $\times 10^{-2}$	(2)	(9.41 ± 0.68) $\times 10^{-3}$	(2)
32	Ge	(6.98 ± 2.8) $\times 10^{-2}$	(2)	(1.71 ± 0.02) $\times 10^{-2}$	(2)
33	As	(2.74 ± 0.87) $\times 10^{-2}$	(2)	(1.85 ± 0.22) $\times 10^{-2}$	(2)
34	Se	(2.19 ± 0.65) $\times 10^{-2}$	(2)	(9.17 ± 0.77) $\times 10^{-3}$	(2)

[a] Assigned uncertainties represents standard deviations from replicate determinations.
[b] Number of replicate determinations.
[c] Monitor cross sections as proposed by Cumming, Ref. 10.

bers between 12 and 34 are given in Table II in groups according to the bombardment energy. The average value, standard uncertainty, and the number of determinations are listed. The data are also displayed graphically in Figs. 1–6.

Special care was taken to eliminate any source of impurity which would lead to exaggerated values for the cross sections. The main errors would arise from trace quantities of the low-Z elements ($12 < Z < 16$) in the target materials for the higher-Z elements ($Z > 22$). In the case of the pellet targets, a blank activity due to the boric acid was measured, and the contribution to the ^{24}Na and ^{22}Na activity was corrected. These corrections ranged from less than 1% for Sc at 300 MeV to 80–100% for the Ga-Se targets at 100 MeV. However, the most conclusive evidence that impurities were negligible, except possibly for the case of high-Z targets at 100 MeV, is the fact that the cross sections decrease markedly with decreasing energy for the higher-Z elements. In fact, the values from As and Se targets were below detection at 100 MeV,

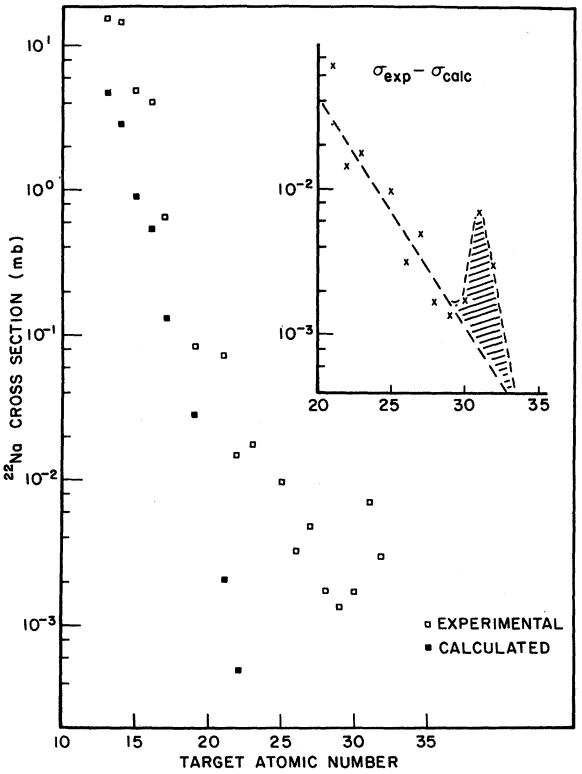

FIG. 1. Production cross sections for ^{22}Na with 100-MeV protons.

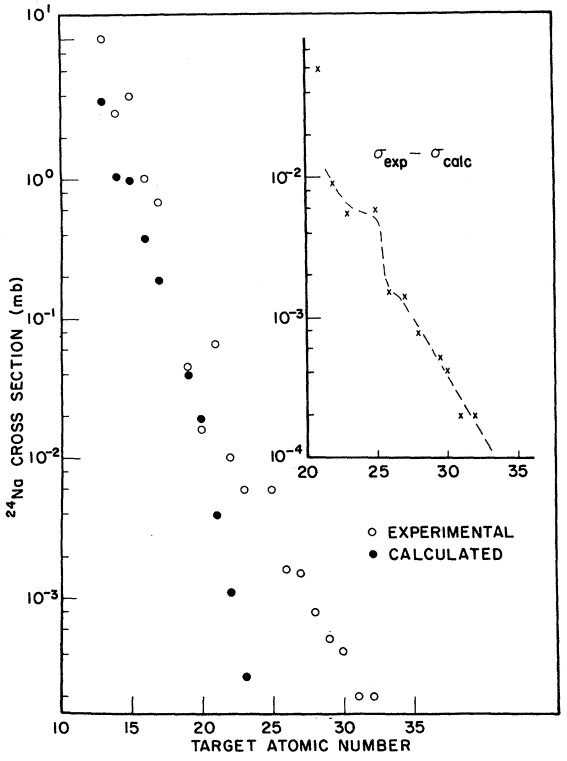

FIG. 2. Production cross sections for ^{24}Na with 100-MeV protons.

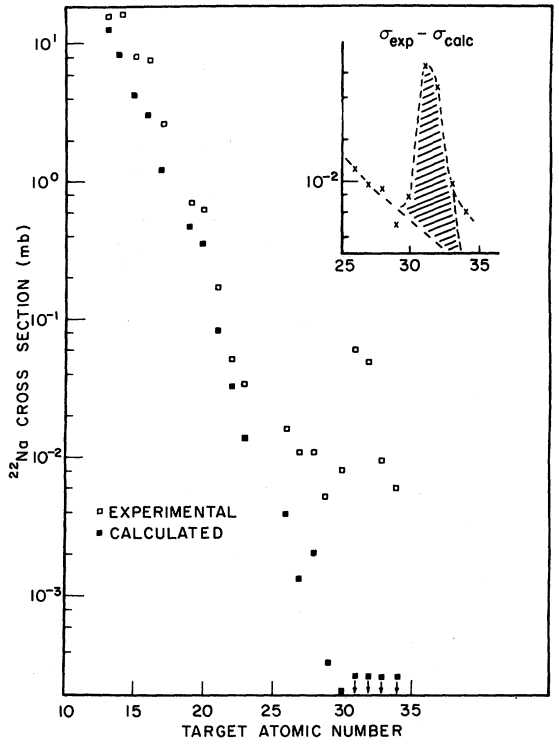

FIG. 3. Production cross sections for ^{22}Na with 200-MeV protons.

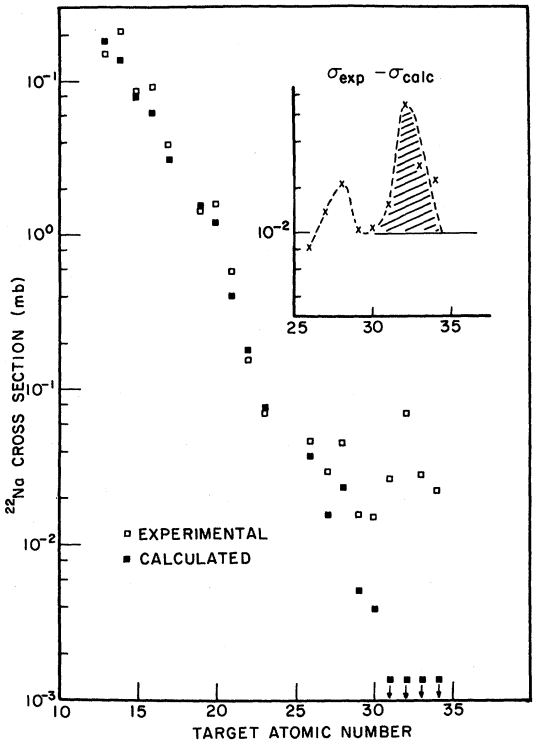

FIG. 5. Production cross sections for ^{22}Na with 300-MeV protons.

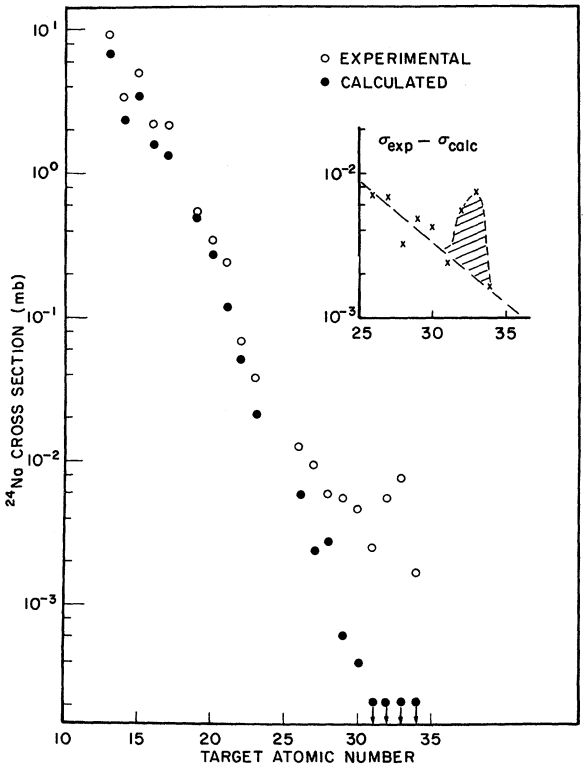

FIG. 4. Production cross sections for ^{24}Na with 200-MeV protons.

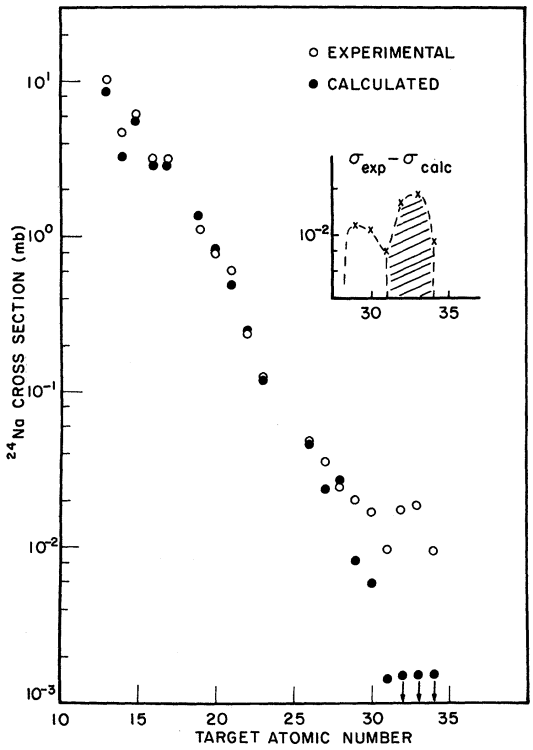

FIG. 6. Production cross sections for ^{24}Na with 300-MeV protons.

indicating no measurable contribution from impurities for these elements once the appropriate corrections had been made. If the observed cross sections were the result of sizable contributions from low-Z elements, the values would have remained relatively constant or perhaps even increased, as the bombardment energy was decreased. It is therefore concluded that the values for the production of ^{24}Na and ^{22}Na, are not in error from these causes, except possibly for the high-Z ($Z > 25$) targets at 100 MeV. Even these values are probably not seriously in error from impurities in view of the behavior of the As and Se cross sections.

Although cross sections for the production of ^{22}Na and ^{24}Na are reported, these values actually represent the sum of the β^- mass chain for ^{24}Na and the β^+ mass chain for ^{22}Na. Hudis[6] has measured the ratio of the ^{24}Ne to ^{24}Na cross sections for a number of elements and at several incident energies. From his data the independent yield for ^{24}Na in the present study is estimated to be $\gtrsim$90% of the values reported. It is expected that a comparable value would be valid for ^{22}Na.

DISCUSSION

The gross exponential decrease of the ^{22}Na and ^{24}Na cross sections as a function of target Z (Figs. 1–8) is the dominant feature of the experimental results with bombarding energies between 100 and 400 MeV. This behavior has been attributed to the cascade-evaporation mechanism.[1,5] However, in addition to the gross exponential decrease, maxima are observed for the production of ^{22}Na and ^{24}Na from targets with $Z > 30$. This feature is not consistent with the conventional cascade-evaporation process. The problem is then to ascertain what proportion of the production cross sections can be attributed to the cascade-evaporation mechanism and what proportion is due to other processes. For simplicity of presentation, the following discussion is separated into the two areas of cascade-evaporation contribution and other processes.

1. Cascade-Evaporation Contribution

Recently, the production of ^{24}Na, ^{22}Na, and ^{18}F has been calculated by Monte Carlo methods assuming a conventional cascade-evaporation mechanism and was shown to agree with the general experimental trends[5] at 300 and 400 MeV from targets between ^{25}Mg and ^{34}S. Both the fluctuations caused by the changing n/p ratio of the target and the general exponential decrease were reproduced. Unfortunately the very small cross sections that have been measured here are not readily calculated by Monte Carlo techniques. However, Rudstam[4] has

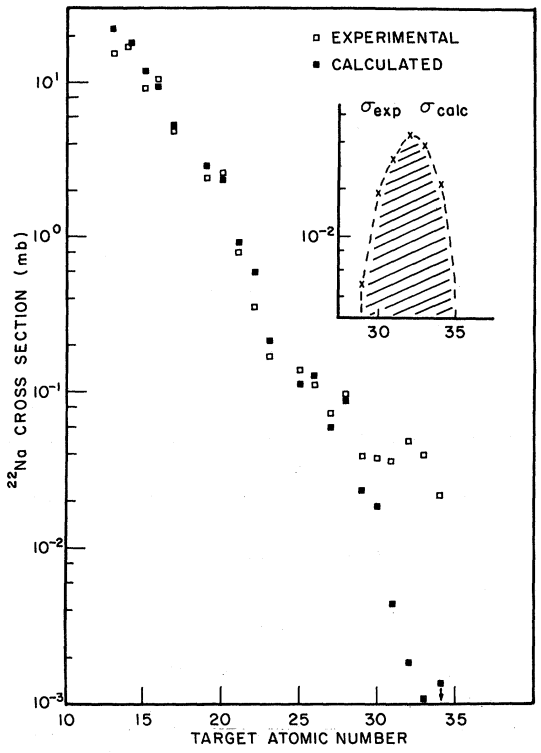

FIG. 7. Production cross sections for ^{22}Na with 400-MeV protons. Data are from Ref. 1.

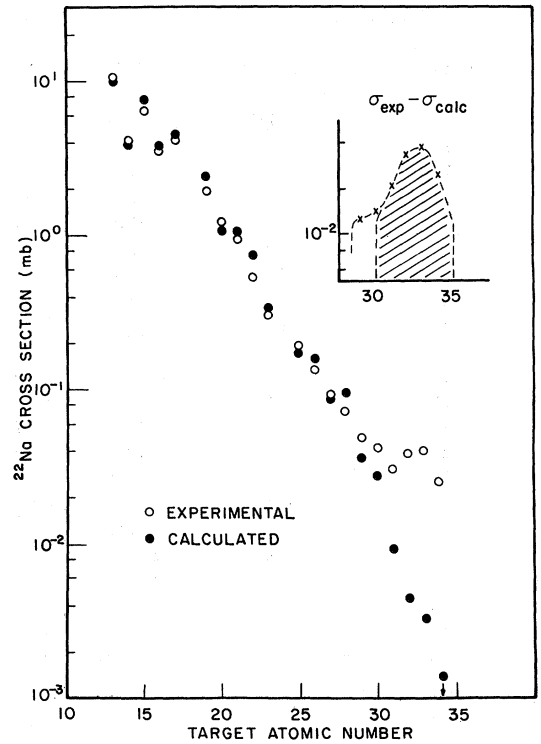

FIG. 8. Production cross sections for ^{22}Na with 400-MeV protons. Data are from Ref. 1.

shown that an analytical function can be used to calculate spallation products. It was therefore decided to apply an analytic function to compare the expected cascade-evaporation Na cross sections with the experimentally determined values.

The Rudstam[4] expression is of the form

$$\sigma(Z,A)=\text{const}\times\exp(PA-R|Z-SA+TA^2|^{3/2}),$$

where P, R, S, and T are experimentally determined parameters. It is immediately obvious that the expression will give a constant value for a ratio between two products as a function of target. This is not consistent with our experimental results as can be seen in Table III and Fig. 9. Since the Rudstam expressions could not be directly applied to the present study, a new expression was developed to represent the production of the Na isotopes.

It was assumed that the form of the new expression was:

$$\sigma(Z,A)=\sigma_g\Gamma_{\Delta A}\Gamma_{Z-Z_A}\Gamma_{N=Z},$$

where σ_g is the geometric reaction cross section for the target, $\Gamma_{\Delta A}$ is the probability of emitting ΔA nucleons, Γ_{Z-Z_A} is the probability of producing nuclide Z in the mass chain A, and $\Gamma_{N=Z}$ is the probability of emitting equal numbers of neutrons and protons in the reaction. It was also assumed that a pseudocompound nucleus was formed for purposes of defining the interaction for the calculation.

The $\Gamma_{\Delta A}$ term must be an exponential and dependent on energy to represent the experimental data.

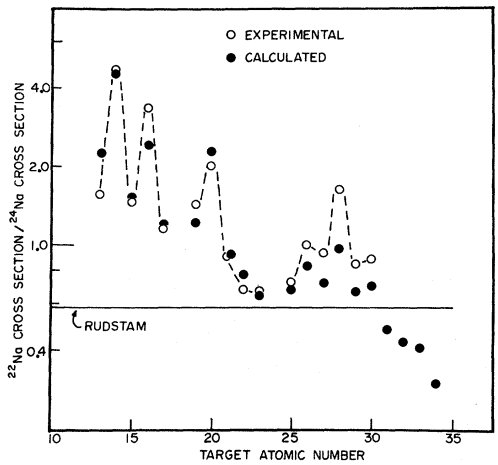

FIG. 9. Comparison of experimental and calculated ratios for the production of ^{22}Na and ^{24}Na. The Rudstam value was calculated from the CDMD expression in Ref. 4.

TABLE III. Ratio of ^{22}Na to ^{24}Na production cross sections.

Target element Atomic number	Symbol	Incident proton energy (MeV) 100	200	300	400[a]	Average[b]	Calculated at 400 MeV
12	Mg[c]	7.34	7.47	6.67	1.31	···	···
13	Al	1.52	1.67	1.54	1.48	1.55	2.26
14	Si	4.97	4.83	4.47	4.16	4.61	4.56
15	P	1.23	1.63	1.52	1.46	1.46	1.53
16	S	4.04	3.35	2.96	2.91	3.32	2.39
17	Cl	0.97	1.22	1.27	1.18	1.16	1.16
19	K	1.88	1.28	1.27	1.26	1.42	1.20
20	Ca	···	1.77	2.00	2.10	1.96	2.31
21	Sc	1.11	0.71	0.96	0.82	0.90	0.90
22	Ti	1.48	0.74	0.63	0.64	0.67	0.77
23	V	2.97	0.90	0.57	0.54	0.67	0.64
25	Mn	1.68	···	···	0.72	0.72	0.67
26	Fe	2.04	1.27	0.93	0.81	1.00	0.83
27	Co	3.36	1.20	0.82	0.77	0.93	0.71
28	Ni	2.14	1.86	1.80	1.33	1.66	0.96
29	Cu	2.68	0.96	0.76	0.79	0.84	0.66
30	Zn	4.09	1.74	0.86	0.91	0.89	0.69
31	Ga	35	24	2.76	1.18	···	0.48
32	Ge	15	8.8	4.08	1.25	···	0.43
33	As	···	1.25	1.48	1.01	···	0.41
34	Se	···	3.61	2.38	0.88	···	0.30

[a]Data from Ref. 1

[b]Average values are for the cases to the right of the solid line. It was assumed that when the ratio changed by more than a factor of 2 for a given element that a process other than the cascade-evaporation mechanism was involved.

[c]Mg was not considered in the calculations since ^{24}Na cannot be formed directly from ^{24}Mg which is the major component of Mg.

The dependence of the ^{24}Na cross section on target mass has been determined by other workers at higher incident energies.[2,3,7] Using the present data and that from the other studies, the slope of the mass dependence can be determined as a function of energy. Specifically, the ^{24}Na cross sections from Al and Cu for $E_p \geq 400$ MeV were normalized[1,5] to the maximum value in the $A = 24$ mass chain. Assuming that ^{24}Na is produced predominantly by the cascade-evaporation mechanism at these energies from these targets, the slope of the mass dependence, $d\ln(^{24}\mathrm{Na})/dA$, can be estimated as a function of incident energy. For energies below 400 MeV the assumption that ^{24}Na is predominantly produced by the cascade-evaporation mechanism from Cu is not necessarily valid. For these energies, the slopes were determined from the present data assuming an exponential dependence fitting the lower mass targets. This mass dependence, P_E, is plotted in Fig. 10 as a function of incident energy.

The similarity between the "P factor" and Rudstam's factor[4] is noteworthy. Using the Rudstam formalism the function can be represented by:

$$P = aE^{-b} \quad \text{for } E < E_0,$$

$$P = c \quad \text{for } E > E_0,$$

where E is the incident energy in MeV, and the constants are given in Table IV. The $\Gamma_{\Delta A}$ term is then of the form $e^{-P\Delta A}$.

The second term, Γ_{Z-Z_A}, which gives the charge distribution for a given mass, was assumed to be of the same form as given by Rudstam[4]:

$$\Gamma_{Z-Z_A} = \exp(-R|Z - SA + TA^2|^{3/2}),$$

where $R = dA^{-c}$.

However, the parameters R, S, and T were found to be different from those determined by Rudstam (see Table V). This is partially due to the fact that the present study is concerned with a lower mass range and partially due to the difference in the over-all expression.

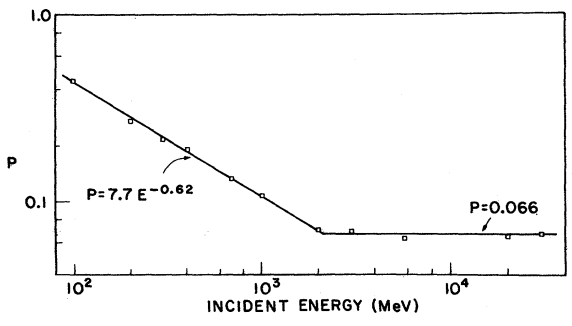

FIG. 10. The energy dependence parameter P determined from the production of ^{24}Na as a function of target mass plotted against incident proton energy. Data are from the present study and Refs. 1–3, 7.

The third term, $\Gamma_{N=Z}$, was included to account for the change in ratio of two products as a function of target. Similar fluctuations have been noted previously[8] and have generally been related to the n/p ratio of the target and product. A recent study of this effect[5] indicated a correlation with the tendency to emit equal numbers of neutrons and protons. The simplest expression to represent this behavior is of the form: $|\Delta A - 2\Delta Z|^2/\Delta A$. It was assumed that this symmetry term was Gaussian in form such that $\Gamma_{N=Z} = \exp(-U|\Delta A - 2\Delta Z|^2/\Delta A)$. Although this function did in fact give the fluctuations that were observed, it was found that the steeper function $\Gamma_{N=Z} = \exp(-U|\Delta A - 2\Delta Z|^{5/2}/\Delta A)$ improved the quantitative fit. However, the fit was not maximized by varying the exponents, although this could easily be done if additional data warranted it.

The determination of U by fitting the data is somewhat arbitrary. Table III indicates that $\sigma(^{22}\mathrm{Na})/\sigma(^{24}\mathrm{Na})$ is essentially constant as a function of energy from those targets where normal cascade and evaporation processes are believed to be dominant. However, the analytic representations of the cascade-evaporation mechanism will predict a change in the ratio as a function of energy, since P is strongly dependent on energy (see the following general expression). The U parameter should also be a function of energy to compensate, but it is not clear why a symmetry term should vary with incident energy. Rather than inserting a purely arbitrary energy dependence into the analytic function, the data were fitted at 400 MeV, and U was found to be equal to 0.55.

The over-all expression is then

$$\sigma(Z,A) = \sigma_g \exp(-P\Delta A - R|Z - SA + AT^2|^{3/2} - U|\Delta A - 2\Delta Z|^{5/2}/\Delta A),$$

where $\sigma_g = \pi(1.26\times10^{-13}A^{1/3})^2$; $\Delta A = A_t + 1 - A$; $\Delta Z = Z_t + 1 - Z$; $U = 0.55$; and P, R, S, and T are given in Tables IV and V. The results of the calculation are given in Table VI and displayed in Figs. 1–9, 11. In general the agreement is good with the exception of the energy dependence of the product ratios. Figure 11 indicates that the parameter P

TABLE IV. Constants defining the parameter P.

	Rudstam[a]		Present study
	CDMD-G	CDMD	
E_0(MeV)	2900	2100	2100
a	13 ± 4	20 ± 7	7.7
b	0.69 ± 0.05	0.77 ± 0.06	0.62
c	0.054 ± 0.002	0.056 ± 0.003	0.066

[a]See Ref. 4.

TABLE V. Constants defining the charge distribution.

	Rudstam[a] CDMD-G	Rudstam[a] CDMD	Present study
d	17.4 ± 4.4	11.8 ± 3.0	11.6
e	0.64 ± 0.07	0.45 ± 0.07	0.45
S	0.487 ± 0.001	0.486 ± 0.001	0.950
T	$(41 \pm 3) \times 10^{-5}$	$(38 \pm 2) \times 10^{-5}$	0.022

[a]See Ref. 4.

might be in error at the lower energies where the ratio of experimental to calculated cross sections is significantly different from 1. However, it does not seem appropriate to correct this error until either further data are available or a clearer understanding of the energy dependence is obtained. At the same time, Fig. 11 indicates that the agreement between experiment and calculation stops at the point where the evaporation chain should cease if the total incident energy were converted to excitation energy and each evaporated nucleon removed 8 MeV.

On the basis of the general agreement of the calculation with the experimental results in the region where the conventional cascade-evaporation mechanism has been shown to hold,[5] it is assumed that the extension of the calculation to the regions where there is no agreement represents, at least semiquantitatively, the contribution of the cascade-evaporation process to the total cross section. The uncertainties in the P factor could change this estimation somewhat, especially at the lowest energies. However, it seems unreasonable to expect a change sufficiently drastic to be able to explain the large differences for targets with $Z \gtrsim 30$. As such, it must be concluded that processes other than the evaporation of nucleons or small clusters of nucleons ($A \lesssim 4$) must be involved in the production of ^{22}Na and ^{24}Na from these higher-Z targets.

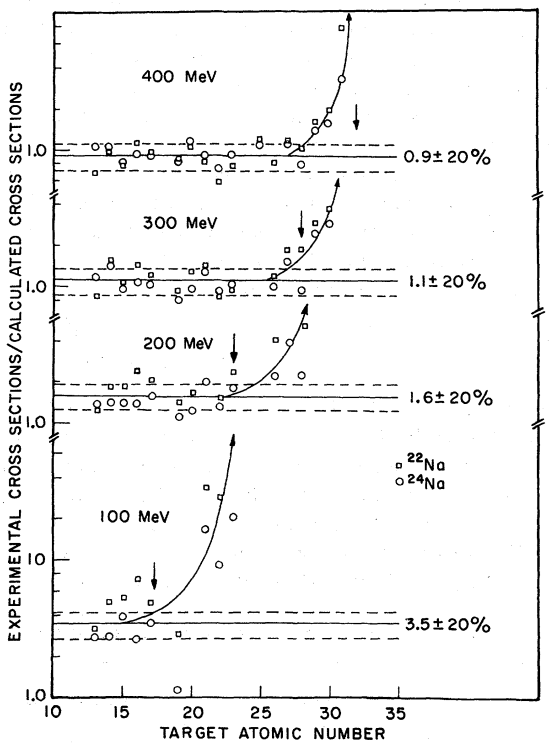

FIG. 11. Comparison of experimental and calculated values for the production of ^{22}Na and ^{24}Na. Arrows indicate the length of a cascade-evaporation chain assuming complete energy transfer and 8 MeV per nucleon binding energy.

2. Other Processes

It is only when the experimental production cross sections deviate from the calculated values that processes other than the conventional cascade-evaporation mechanism are important in the production of these products. Assuming then that these deviations are due to other processes, an estimate of their contributions to the production of the Na isotopes can be made (see Figs. 1–8). Figure 12 illustrates the comparison for Cu. The cascade-evaporation contribution is seen to rise rapidly with increasing energy, as is to be expected. The contribution from "other" processes also rises rapidly with energy, but it has a much lower threshold value (≲100 MeV) and levels off above 200 MeV. From this information the "other" pro-

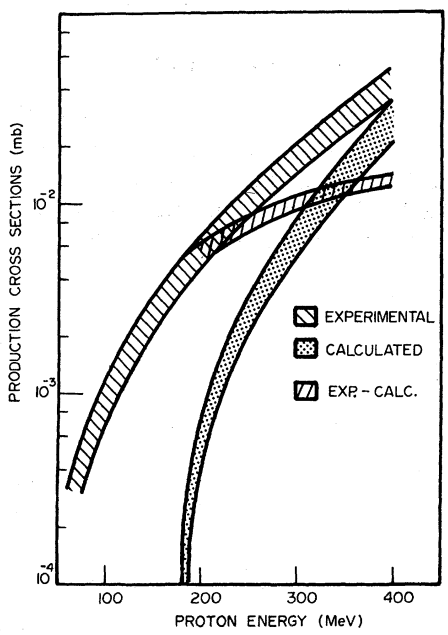

FIG. 12. Excitation functions for the production of ^{22}Na or ^{24}Na from Cu. The width of the bands include the values for both ^{22}Na and ^{24}Na production.

TABLE VI. Production cross sections for ^{22}Na and ^{24}Na.

Target atomic number	^{22}Na Calc.	^{22}Na Exp.	^{22}Na Exp./Calc.	^{24}Na Calc.	^{24}Na Exp.	^{24}Na Exp./Calc.
			100-MeV incident protons			
13	4.87	15.5	3.18	3.59	10.2	2.84
14	2.86	14.5	5.07	1.05	2.92	2.78
15	0.907	4.90	5.40	0.994	3.98	4.00
16	0.548	4.08	7.45	0.381	1.01	2.65
17	0.130	0.649	4.99	0.188	0.669	3.56
19	2.86×10^{-2}	8.39×10^{-2}	2.93	3.96×10^{-2}	4.46×10^{-2}	1.13
20	1.83×10^{-2}	...	...	1.93×10^{-2}	1.59×10^{-2}	0.82
21	2.06×10^{-3}	7.30×10^{-2}	35.4	3.84×10^{-3}	6.60×10^{-2}	17
22	4.93×10^{-4}	1.48×10^{-2}	30.0	1.06×10^{-3}	1.00×10^{-2}	9.4
23	1.01×10^{-4}	1.77×10^{-2}	1.8×10^{2}	2.74×10^{-4}	5.96×10^{-3}	22
25	1.93×10^{-5}	9.8×10^{-3}	5.1×10^{2}	4.77×10^{-5}	5.84×10^{-3}	1.2×10^{2}
26	1.74×10^{-5}	3.21×10^{-3}	1.8×10^{2}	3.49×10^{-5}	1.57×10^{-3}	45
27	3.64×10^{-6}	4.98×10^{-3}	1.4×10^{3}	8.60×10^{-6}	1.48×10^{-3}	1.7×10^{2}
28	5.88×10^{-6}	1.71×10^{-3}	2.9×10^{2}	1.02×10^{-5}	7.98×10^{-4}	78
29	4.37×10^{-7}	1.36×10^{-3}	3.1×10^{3}	1.10×10^{-6}	5.08×10^{-4}	4.6×10^{2}
30	2.17×10^{-7}	1.71×10^{-3}	7.9×10^{3}	5.21×10^{-7}	4.18×10^{-4}	8.0×10^{2}
31	1.4×10^{-8}	7.0×10^{-3}	5×10^{5}	4.9×10^{-8}	2.0×10^{-4}	4.1×10^{3}
32	2.8×10^{-9}	3.0×10^{-3}	1×10^{6}	1.1×10^{-8}	2.0×10^{-4}	1.8×10^{4}
33		...			...	
34		...			...	
			200-MeV incident protons			
13	12.4	15.5	1.25	6.69	9.3	1.39
14	8.65	16.1	1.86	2.32	3.33	1.44
15	4.31	8.01	1.86	3.45	4.91	1.42
16	3.08	7.36	2.39	1.57	2.20	1.40
17	1.24	2.60	2.10	1.31	2.14	1.63
19	0.482	0.691	1.43	0.489	0.538	1.10
20	0.360	0.606	1.68	0.275	0.343	1.25
21	8.66×10^{-2}	0.17	1.96	0.118	0.24	2.03
22	3.27×10^{-2}	5.04×10^{-2}	1.54	5.17×10^{-2}	6.82×10^{-2}	1.32
23	1.41×10^{-2}	3.40×10^{-2}	2.41	2.06×10^{-2}	3.78×10^{-2}	1.83
25	3.84×10^{-3}	...	...	6.94×10^{-3}	...	...
26	3.98×10^{-3}	1.64×10^{-2}	4.12	5.86×10^{-3}	1.29×10^{-2}	2.20
27	1.35×10^{-3}	1.09×10^{-2}	8.07	2.33×10^{-3}	9.12×10^{-3}	3.91
28	2.10×10^{-3}	1.10×10^{-2}	5.23	2.67×10^{-3}	5.91×10^{-3}	2.21
29	3.32×10^{-4}	5.25×10^{-3}	16	6.11×10^{-4}	5.46×10^{-3}	8.94
30	2.20×10^{-4}	8.04×10^{-3}	36	3.87×10^{-4}	4.61×10^{-3}	12
31	2.81×10^{-5}	6.0×10^{-2}	2.1×10^{3}	7.15×10^{-5}	2.47×10^{-3}	34
32	8.61×10^{-6}	4.9×10^{-2}	5.7×10^{3}	2.5×10^{-5}	5.57×10^{-3}	2.2×10^{2}
33	4.08×10^{-6}	9.5×10^{-3}	2.3×10^{3}	1.20×10^{-5}	7.63×10^{-3}	6.4×10^{2}
34	4.10×10^{-7}	6.9×10^{-3}	1.5×10^{4}	1.66×10^{-6}	1.66×10^{-3}	1.0×10^{3}
			300-MeV incident protons			
13	18.2	15.5	0.85	8.62	10.1	1.17
14	13.7	20.8	1.52	3.21	4.65	1.45
15	8.15	8.42	1.03	5.74	5.53	0.96
16	6.23	9.05	1.45	2.80	3.06	1.09
17	3.13	3.84	1.23	2.91	3.03	1.04
19	1.54	1.40	0.91	1.37	1.10	0.80
20	1.22	1.57	1.29	0.827	0.784	0.95
21	0.402	0.58	1.44	0.481	0.60	1.25
22	0.182	0.149	0.82	0.254	0.237	0.93
23	7.32×10^{-2}	7.16×10^{-2}	0.98	0.122	0.125	1.02
25		...			...	
26	3.69×10^{-2}	4.50×10^{-2}	1.22	4.79×10^{-2}	4.84×10^{-2}	1.01
27	1.53×10^{-2}	2.88×10^{-2}	1.88	2.32×10^{-2}	3.50×10^{-2}	1.51

TABLE VI (*Continued*)

28	2.35×10^{-2}	4.46×10^{-2}	1.90	2.63×10^{-2}	2.48×10^{-2}	0.94
29	5.05×10^{-3}	1.51×10^{-2}	2.99	8.19×10^{-3}	1.98×10^{-2}	2.42
30	3.76×10^{-3}	1.46×10^{-2}	3.88	5.83×10^{-3}	1.69×10^{-2}	2.90
31	6.32×10^{-4}	2.60×10^{-2}	41	1.42×10^{-3}	9.41×10^{-3}	6.63
32	2.36×10^{-4}	6.98×10^{-2}	2.96	5.98×10^{-4}	1.71×10^{-2}	29
33	1.29×10^{-4}	2.74×10^{-2}	2.1×10^{2}	3.34×10^{-4}	1.85×10^{-2}	55
34	1.68×10^{-5}	2.19×10^{-2}	1.3×10^{3}	5.95×10^{-5}	9.17×10^{-3}	1.5×10^{2}
			400-MeV incident protons[a]			
13	22.5	15.5	0.69	9.94	10.5	1.06
14	17.6	17.4	0.99	3.86	4.18	1.08
15	11.7	9.39	0.80	7.65	6.44	0.84
16	9.29	10.4	1.12	3.88	3.58	0.92
17	5.26	4.88	0.93	4.55	4.14	0.91
19	2.94	2.45	0.83	2.44	1.95	0.80
20	2.43	2.56	1.05	1.05	1.22	1.16
21	0.952	0.786	0.83	1.06	0.959	0.91
22	0.580	0.344	0.59	0.751	0.538	0.72
23	0.215	0.166	0.77	0.336	0.307	0.91
25	0.114	0.136	1.19	0.169	0.190	1.12
26	0.130	0.108	0.83	0.156	0.133	0.85
27	5.99×10^{-2}	7.13×10^{-2}	1.19	8.47×10^{-2}	9.21×10^{-2}	1.09
28	9.13×10^{-2}	9.58×10^{-2}	1.05	9.50×10^{-2}	7.18×10^{-2}	0.76
29	2.33×10^{-2}	3.81×10^{-2}	1.64	3.52×10^{-2}	4.81×10^{-2}	1.37
30	1.85×10^{-2}	3.75×10^{-2}	2.03	2.67×10^{-2}	4.10×10^{-2}	1.54
31	4.42×10^{-3}	3.53×10^{-2}	7.99	9.20×10^{-3}	2.98×10^{-2}	3.24
32	1.83×10^{-3}	4.68×10^{-2}	26	4.30×10^{-3}	3.76×10^{-2}	8.74
33	1.08×10^{-3}	3.98×10^{-2}	37	2.61×10^{-3}	3.95×10^{-2}	15
34	1.62×10^{-4}	2.19×10^{-2}	1.35	5.39×10^{-4}	2.49×10^{-2}	46

[a]Experimental data is from Ref. 1.

cesses, in the case of Cu, seem to be relatively low-energy processes which reach their maxima by ~200 MeV. The steep excitation functions,[2,3,7] which have been measured previously for these products, are then mainly a result of the rapid increase of the cascade-evaporation process, and are not necessarily associated with the processes responsible for the anomalously high cross-sectional values.

Attention should also be drawn to the energetics of these reactions. If the cascade-evaporation mechanism is to describe the production of these Na isotopes from targets in the region of Ni and Cu, a total of ~40 nucleons must be emitted predominantly as individual particles. At the low bombarding energies of 100, 200, and even 300 MeV, this would mean that, on the average, each nucleon was emitted with less than its binding evergy, even if the total energy of the incident proton was converted into excitation energy of the nucleus. Such a prospect seems highly unlikely. However, if either light fragments ($A>4$) were predominantly emitted or, what is more likely, the nucleus were divided into two large fragments with a few nucleons also being emitted, the energy conditions could be met.

One of the most interesting aspects of these results is the peaks or maxima observed in the distributions of fragments as a function of target. These maxima, as illustrated in the present results and in those at 400 MeV,[1] occur for values of $Z\simeq 31-34$, 42–47, and $N\simeq 40-45$, 52–60. The positions of the maxima must be related in some unique way to the measured products. If a major breakup were responsible for the formation of these products, as energetic considerations would suggest, the complimentary fragment would need to have $Z\gtrsim 20-23$, 31–35, and $N\lesssim 27-34$, 38–49 depending upon the specific product and maxima. It is interesting to note that these ranges for the mass of the complimentary fragments are just in excess of those for the stable configurations of 20 and 28 for protons and 28 for neutrons. It seems possible, therefore, that these stable configurations are involved.

The results at 100 MeV suggest an additional maximum. Energetically, a maximum of 10 to 12 individual nucleons would be expected to be emitted with 100 MeV incident protons, and the total mass loss could be perhaps twice that amount if α particles and similar fragments are also emitted. This would mean that the production cross sections of the Na isotopes with 100-MeV protons from targets with $A\gtrsim 40$ should rapidly go to zero. This is

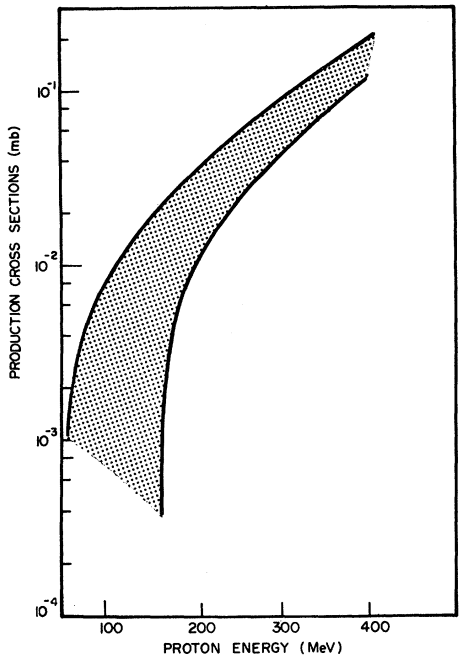

FIG. 13. Excitation function for the production of ^{22}Na and ^{24}Na from the maxima at $Z \simeq 32$. The width of the band includes the values for the shaded areas in Figs. 1–8 for both ^{22}Na and ^{24}Na production.

not observed to happen. In fact, a shoulder seems to appear in this region (see Figs. 1 and 2). If these values are correct, and we have no reason to doubt them, they imply another maximum in the distribution with a range of $Z \simeq 20$–23 and $N \simeq 20$–28. Thus, if the production of the Na isotopes from this region with 100-MeV protons is by the formation of two large fragments, as suggested by energy considerations, then the complimentary fragment would have $Z \sim 9$–12 and $N \sim 9$–15. Again the proximity to the stable configurations of Z and $N = 8$ can be noted.

An estimate of the excitation function for the maximum at $31 \lesssim Z \lesssim 34$ is given in Fig. 13. As in the Cu case, the cross sections for this "other" process responsible for the maximum is seen to rise rapidly with energy and to have a relatively low threshold value ($\lesssim$100 MeV). Again it seems that a primarily low-energy process is responsible. Clearly some form of large-fragment breakup must be involved.

It is difficult to postulate any specific mechanism by which breakup processes of the type suggested here could take place. Makarov *et al.*[9] have found it necessary to postulate preformed clusters in order to account for the light-fragment ($Z \lesssim 7$) angular distribution and asymmetry that they observed in photographic emulsions. It cannot be decided solely from the data reported here whether the present processes involve an interaction with a preformed nuclear cluster, or whether somewhat more conventional evaporation processes are involved in which the Na cross sections are enhanced because of the greater stability of one of the evaporation fragments. Clearly, additional work will be necessary to understand the mechanism for the production of fragments such as Na from targets with $Z \gtrsim 30$ and at energies less than 500 MeV.

CONCLUSIONS

Considering all of the characteristics of these distributions, the most likely and most consistent description of the data requires the combination of at least two different processes. The first is that of the conventional cascade-evaporation model which gives rise to the exponential form of the distributions. This process can be represented by an analytic function and calculated.[10] The second is a breakup of the nucleus into two large fragments with the likelihood of a few nucleons or groups of nucleons also being emitted. This second process gives rise to maxima in the distribution and can be correlated with relatively stable configurations as the complimentary fragments to the ones which result in the measured Na isotope. However, further work is required to substantiate and to elucidate these "other" processes.

ACKNOWLEDGMENTS

We wish to express our appreciation to the staff at Carnegie-Mellon University for making it possible for one of us (R.G.K.) to visit and use the facilities of their nuclear research center where a major share of the experimental work was accomplished. We also wish to thank Gary Smay for miscellaneous assistance in data processing.

---

*Work sponsored by the U. S. Atomic Energy Commission and the National Research Council of Canada.

[1]R. G. Korteling and A. A. Caretto, Jr., J. Inorg. Nucl. Chem. 29, 2863 (1967).

[2]A. A. Caretto, Jr., J. Hudis, and G. Friedlander, Phys. Rev. 110, 1130 (1958).

[3]V. P. Crespo, J. M. Alexander, and E. K. Hyde, Phys. Rev. 131, 1763 (1963).

[4]G. Rudstam, Z. Naturforsch. 21, 1027 (1966).

[5]R. G. Korteling and A. A. Caretto, Jr., Phys. Rev. C. 1, 193 (1970).

[6]J. Hudis, Phys. Rev. 171, 1301 (1968).

[7]J. Hudis, I. Dostrovsky, G. Friedlander, J. R. Grover, N. T. Porile, L. P. Remsberg, R. W. Stoenner, and S. Tanaka, Phys. Rev. 129, 434 (1964).

[8]I. Dostrovsky, R. Davis, Jr., A. M. Poskanzer, and P. L. Reeder, Phys. Rev. 139, B1513 (1965).

[9]M. M. Makarov, Zh. Eksperim. i Teor. Fiz. 45, 56 (1963) [transl.: Soviet Phys.–JETP 18, 41 (1964)].

[10]J. B. Cumming, Ann. Rev. Nucl. Sci. 13, 261 (1963).